Published in final edited form as:
J Phys Chem Lett. ; 5(1): 212–219. doi:10.1021/jz4025386.

Vibrational Excitations and Low Energy Electronic Structure of Epoxide-decorated Graphene

E.C. Mattson[1,*], **J.E. Johns**[2], **K. Pande**[1], **R.A. Bosch**[3], **S. Cui**[4], **M. Gajdardziska-Josifovska**[1], **M. Weinert**[1], **J.H. Chen**[4], **M.C. Hersam**[5,6], and **C.J. Hirschmugl**[1,*]

[1]University of Wisconsin-Milwaukee, Physics Dept., Milwaukee, WI 53211

[2]University of Minnesota, Chemistry Dept, Minneapolis, MN 55455

[3]Synchrotron Radiation Center, University of Wisconsin-Madison, Stoughton, WI 53589

[4]University of Wisconsin-Milwaukee, Mechanical Engineering Dept., Milwaukee, WI 53211

[5]Northwestern University, Chemistry Dept., Evanston, IL 60208

[6]Northwestern University, Materials Science and Engineering Dept., Evanston, IL 60208

Abstract

We report infrared studies of adsorbed atomic oxygen (epoxide functional groups) on graphene. Two different systems are used as a platform to explore these interactions, namely, epitaxial graphene/SiC(0001) functionalized with atomic oxygen (graphene epoxide, GE) and chemically reduced graphene oxide (RGO). In the case of the model GE system, IR reflectivity measurements show that epoxide groups distort the graphene π bands around the K-point, imparting a finite effective mass and contributing to a band gap. In the case of RGO, epoxide groups are found to be present following the reduction treatment by a combination of polarized IR reflectance and transmittance measurements. Similar to the GE system, a band gap in the RGO sample is observed as well.

Keywords

epitaxial graphene; oxygen; adsorbates; vibrations; band structure; reduced graphene oxide

The isolation of graphene[1] and subsequent experiments detailing its unusual properties [2, 3] have revolutionized the field of materials science. Many astounding physical properties derived from its unusual electronic structure have been discovered[4] and sparked widespread interest; however, important directions in graphene research involve developing methods for incorporating graphene into devices, and modification such that it may be tailored to a particular application. Just as Si-based devices rely heavily on doping, chemical modification, and interfacing with other materials, pristine graphene must also be functionalized or chemically activated in order to become economically viable in applications such as electronics, electrochemical energy storage, catalysis, and sensing. Decoration of graphene with adatoms,[5–7] molecules,[8] nanocrystals[9–12] and self-assembled monolayers[13] have all been demonstrated; however, controllable chemical modification of graphene through doping and adsorption while maintaining acceptable transport properties remains challenging since pristine graphene is quite inert.

*Corresponding Authors: emattson@uwm.edu, cjhirsch@uwm.edu.

Chemical oxidation is a promising route but often results in deleterious and irreversible effects on the substrate. However, recent advances have demonstrated the possibility of reversible oxidation of graphene under highly controlled conditions using atomic oxygen. Chemisorbed atomic oxygen on the basal plane of graphene occupies the carbon bridge site, forming an epoxide group. Decorating graphene with epoxide groups yields a reactive surface,[8, 14] and is predicted to result in the opening of a band gap.[15–17] Epoxide groups can also act as nucleation centers for the subsequent growth of metal oxide clusters and nanocrystals.[18] Thus, it is critical to identify characteristic markers of epoxide groups on graphene and understand their effect on its electronic structure.

Here we consider two systems in which graphene is functionalized with epoxide groups. First, we study EG/SiC(0001) oxidized with an atomic oxygen source in ultra-high vacuum, creating graphene epoxide (GE).[5] This well-defined system has been extensively characterized and found to be chemically homogeneous and controllable. Second, we investigate RGO, a material that is becoming increasingly popular for many applications due to its versatility and low-cost production from graphene oxide (GO).[19–21] Synchrotron-based infrared reflectance and transmittance measurements are performed to study both low-energy electronic structure and vibrational fingerprints of adsorbed species. We report the vibrational frequencies of individual epoxide groups on EG/SiC(0001) and demonstrate that these groups open a small gap of ≈0.28 eV. In the case of RGO, we clarify the origin of the IR signals observed in previous studies as arising from vibrations of residual epoxide groups on the graphene basal planes. Similar to the model GE, epoxide groups in RGO open a band gap (≈0.19 eV) and are responsible for its semiconducting properties.

Fig. 1A shows a reflectivity spectrum taken from the Si-face of the clean EG sample referenced to that of a clean $6\sqrt{3} \times 6\sqrt{3}$ SiC(0001) substrate. Several vibrational absorption features are observed. The strongest feature in the spectrum is an intense, asymmetric feature spanning ≈850–1100 cm^{-1}, which is assigned to the previously-observed surface plasmon-polariton (SPP).[22] This resonance arises due to the coupling of the free carriers in EG to the SiC phonon mode in the region where its refractive index becomes negative, resulting in a reflection enhancement. An additional feature with a characteristic Fano lineshape is observed at 1590 cm^{-1} due to the C=C stretching mode. For a pristine graphene sample, this mode is forbidden by symmetry but becomes active in the event of symmetry breaking between the two sublattices,[23–25] such as asymmetric interactions with the SiC buffer layer.

Fig. 1B shows the reflectivity spectrum of GE referenced to that of EG, with a focus on the fingerprint region shown in Fig. 1C. The epoxide coverage is ≈3%, determined from scanning tunneling microscopy imaging. The appearance of a feature at 1620 cm^{-1} indicates a blueshift of the C=C stretching mode; note that since the reflectance curve here is referenced to (divided by) that of the EG, the observed position at 1620 cm^{-1} is not necessarily indicative of the actual center frequency of the mode. Nevertheless, the feature does clearly indicate a blueshift of the C=C mode, which could be explained by the formation of an sp^3 bonding configuration formed within at least a fraction of the sample and is similar to the C=C stretching frequencies observed for graphene oxide.[26–29] A shift of the Fermi level induced by the oxidation could also play a role in the observed peak shift; previous studies of gated exfoliated bilayer graphene showed significant modulations of the lineshapes and frequencies of the C=C mode as a function of gating,[23, 25] and moving away from charge-neutrality ultimately results in a softening of the C=C mode.[23] Such a shift is consistent with a hole-doping effect resulting from the oxidation. In the region 1720–1900 cm^{-1}, several bands are observed and assigned to carbonyl groups arising from oxidation of the underlying SiC substrate. We emphasize that STM imaging of the graphitized layers has indicated a chemically homogeneous distribution of oxygen in the form of epoxide groups,

and not carbonyl groups. Further assignment of these bands is beyond the scope of the current work. A broad absorption band is observed between 1100–1400 cm^{-1}, centered at 1285 cm^{-1}; this feature is assigned to superimposed modes associated with the symmetric and asymmetric epoxide C-O-C bond stretching. Because oxygen is nearly identical in mass to carbon, the fundamental translations expected for an atomic adsorbate couple strongly to the phonon modes of the substrate. This results in significant vibrational dephasing and shortening of the vibrational lifetime, producing a substantially broader absorption profile than that observed for the C=C stretching mode. It is difficult to estimate the vibrational lifetime based on the peak width because the spectral region of interest involves a superposition of more than one mode, and there is a significant modulation of the baseline at the low-wavenumber region of the band. The band centered at 1490 cm^{-1} is assigned to C=C stretching of the C atoms hosting the epoxide oxygen atom; this mode also involves a distortion of the C-O-C bond angle and a c-axis displacement of the oxygen atom, resulting in a frequency lower than that of the C=C stretching in the unoxidized carbon atoms.

We next consider the broadband characteristics of the reflectivity of EG and GE. The EG/SiC system is highly electron doped, with the Fermi level lying between 0.35-0.4 eV above the Dirac point.[30, 31] Consequently, all interband optical transitions should be suppressed below the optical transition threshold of 0.7–0.8 eV. The spectrum in Fig. 1A, shows enhanced reflectivity near the SPP, which gradually decreases with increasing energy until it reaches its minimum value at ≈4800 cm^{-1} (0.6 eV), at which point it begins continuously increasing. To carefully interpret the origin of these features, we extracted the optical conductivity of the graphitized layers using a Kramers-Kronig consistent fitting program,[32] taking into account the substrate. In the extracted optical conductivity of the clean graphene sample (Fig. 2A), two clear absorption thresholds are observed. The transition onset at 4800 cm^{-1} (0.6 eV) corresponds to the $2|E_f|$ interband absorption threshold of graphene.[33, 34] Interestingly, there is also a clear broadband absorption feature from 1500 to 3000 cm^{-1}. Previous photoemission studies on epitaxial graphene have reported the presence of a band gap of approximately 0.25 eV at the K-point,[30, 31, 35] although this gap is well below the Fermi level and therefore is not responsible for the feature observed here. A study of the 0th order (buffer) and 1st order graphene layers on SiC(0001) found that the buffer layer ($6\sqrt{3} \times 6\sqrt{3}$ SiC(0001) reconstruction) is effectively a warped graphene layer in which the graphene symmetry is broken by bonding with the substrate.[36] Band structure calculations of the 1st graphene layer + buffer layer indicated that, due to the interaction with the buffer layer, the 1st graphene layer is distorted around the K-point, which accounts for the photoemission results reporting a band gap of 0.25 eV.[30, 31, 35] The calculations predict that the presence of the buffer layer leads to additional bands around the K-point, within about 0.3 eV of the Fermi level.[36] This results in additional allowed direct interband transitions between bands around the K-point that could be responsible for the feature observed in the infrared measurements shown here.

Relative to the clean EG sample, the GE sample demonstrates a significant modulation of the broadband reflectance. In the low-energy region (<3000 cm^{-1}) the reflectance is lower than that of the clean EG; there is a reflectivity threshold at ≈2000 cm^{-1}, at which point the reflectivity begins increasing, exceeding that of the clean sample >3000 cm^{-1}, and increasing continuously to the high frequency limit of the present measurement. The real part of the conductivity, obtained from the ratio of the reflectivity GE to clean EG, is shown in Fig. 2B. As with the reflectivity spectra, there is a threshold at 2000 cm^{-1}, and the conductivity of GE ultimately increases to nearly 3 times that of EG. Above 5000 cm^{-1}, where the conductivity of EG begins increasing, the ratio decreases slightly and appears to level off at ~1.7.

The relative increase of the conductivity can be explained by a distortion of the electronic band structure induced by the epoxide groups. The optical properties of free-standing graphene are well-described by the joint-density-of-states (JDOS) of a two-dimensional semiconductor, where the optical conductivity is a step function at $2|E_f|$.[32, 33] The case of EG is more complicated due to the multilayer structure including the substrate, buffer layer, and subsequent graphene layers; thus the electronic properties of this system cannot be adequately accounted for by a 2D model. Rather, we consider the JDOS of a 3D material within the vicinity of an M_o-type critical point:[37]

$$D_{cv}(\hbar\omega)=\frac{1}{2\pi^2}\left(\frac{2\mu}{\hbar^2}\right)^{3/2}(\hbar\omega-\varepsilon_g)^{1/2} \quad \text{Eq. (1)}$$

Here hstrok; is Planck's constant divided by 2π, ω the photon frequency, ε_g the magnitude of the energy gap, and μ the reduced mass: $\mu=\frac{m_c m_v}{m_c+m_v}$, for the band masses of the valence and conduction bands m_v and m_c, respectively. The conductivity is proportional to the JDOS weighted by the dipole matrix element connecting the initial and final states.[37] The electrons occupying the π states in graphene behave as "massless Dirac fermions" [2, 38] because the linear dispersion around the K-point implies zero effective mass. The increased relative conductivity of the O-dosed sample relative to the clean sample implies an increase of either the effective mass, the dipole matrix element, or both of these. However, the matrix element connecting the valence and conduction states is generally approximated as being inversely proportional to the effective mass, resulting in a more intense transition for lighter charge carriers. Therefore, the increase in the transition strength of the O-dosed sample suggests a greater effective mass of the charge carriers. Any curvature induced in the π bands will impart a nonzero effective mass to the charge carriers, resulting in an enhancement of the optical transitions.

Of particular interest is the softening of the interband absorption threshold. The differential reflectance spectrum R_{GE}/R_{EG} shows an onset at ≈2200 cm^{-1}, whereas the absorption threshold for the clean EG was observed at >5000 cm^{-1}. This indicates the presence of available transitions in GE at lower energies than that observed for the EG. This could be indicative that a band gap has been opened, or the sample is simply hole-doped with a lower energy of the transition threshold. Close inspection of the absorption onset in the reflectivity spectra suggests the former is the case. At the frequency of the absorption onset, there is a discontinuity in the slope of the reflectivity (black overlay in Fig. 1C), at which point the reflectivity begins to increase slowly and continuously, characteristic of the JDOS around an M_o-type critical point. This is in contrast to the steep threshold observed for clean graphene, both here (> 4800 cm^{-1} in Figs. 1A and 2A) and in other work.[33, 34, 39] In combination, the shape of the discontinuity and the absorption threshold strongly suggest that the Fermi level lies within the gap and the van Hove singularity in the JDOS is accessible with our optical measurement. Based on the position of the discontinuity, the gap can be estimated as 2250 cm^{-1} (≈0.28 eV). The origin of the decreased conductivity/reflectivity of GE below 3000 cm^{-1} (≈0.3 eV, where the ratio=1 in Figs. 1B and 2B) relative to that of the EG sample can be attributed to a hole-doping of the sample such that the states associated with the buffer layer lie above E_f. The central conclusions drawn from these spectra are shown in Fig. 2C, which illustrates schematic band diagrams of the clean and oxidized systems.

From the conductivity spectra, we can additionally conclude that the measured gap in the GE results from chemical interactions, and not from a rigid band shifting of the EG band structure. It has been reported that monolayer EG (the 1st order layer) has an apparent band gap ~0.25 eV due to its interaction with the substrate;[30, 40] thus, it is reasonable to ask whether the gap that we measure is derived from simple hole doping to expose the gap that

is reportedly inherent to EG. For example, it was observed[40] that dosing EG with NO_2 causes a rigid downward shift of the entire band structure to bring the valence band maximum below the Fermi level and render the sample a semiconductor. In contrast to this effect, the continuous increase of the conductivity/reflectivity in our data (Figs. 1B and 2B) is inconsistent with a rigid shift of the entire band structure and rather suggest a distortion of the valence and conduction bands due to covalent bonding with oxygen. Furthermore, the band gap induced in bilayer graphene by electrostatic doping monotonically increases with increasing field strength. By the lowering the electron concentration through p-type dopants, a purely electrostatic model would predict a lowering of the band gap.[41] This result could potentially be utilized for graphene-based applications, as it is demonstrated that the epoxide decoration can be used to tune the electronic properties of graphene in a controlled way. Furthermore, unlike the case for NO_2 adsorption, the chemical bond between the carbon and oxygen atoms is thermally robust and stable at room temperature[5] whereas desorption of NO_2 from graphite occurs at 140 K.[42]

Based on insights derived from the model GE system, we now consider another system, RGO, which we argue below consists of epoxide-deocrated graphene. Despite being structurally defective, RGO offers an inexpensive and scalable route toward production of graphene-based materials[43] and composites.[10, 11, 44, 45] Numerous reports characterizing the product obtained by reduction of GO demonstrate that the specific oxidation and reduction treatments used can impact the resulting characteristics of RGO. In addition, there have been multiple discrepancies in the literature regarding the assignments of IR bands.[27, 28, 46–48] Identification of the species in RGO is critical, as different species have different effects on its electronic structure, reactivity and overall properties. We now consider the composition and geometric structure of the residual oxygen in RGO prepared by hydrazine reduction. Fig. 3A shows an absorbance spectrum generated from an unpolarized transmission measurement of an RGO sample on a diamond substrate. In the fingerprint region, 3 bands are clearly resolved.

At 1730 cm^{-1}, an intense band is observed due to C=O stretching of carbonyl groups. These groups are only present at regions in which the hexagonal carbon network is disrupted, such as edges and vacancies, since two electrons are needed to form the C=O bond. The band at 1580 cm^{-1} is due to the C=C stretching mode of the underlying lattice. The most controversial feature is the intense mode spanning the region from 1050–1350 cm^{-1}. Many other works have observed a feature in the same frequency region,[27, 46, 48] and Acik et. al.[27] assigned similar features in thermally-reduced GO to edge ether moieties based on first-principles calculations. Differentiation between ether and epoxide modes for such features is difficult, however, since both functional groups involve the stretching modes of C-O-C bonds. To rule out the possibility that this mode originates from a nitrogen functional group persisting following the hydrazine treatment, we performed a similar absorption measurement on thermally-reduced GO (supplemental information) and found very similar results.

We can distinguish between these groups by considering the atomic displacements associated with the C-O-C modes in both cases. Fig. 3B shows the normal modes for the epoxide group in analogy with the modes of a bridge-bonded atomic adsorbate on a surface in which the substrate atoms are frozen. The three translational degrees of freedom of the adsorbate now become modes that are predominantly asymmetric stretching (ν_{as}), symmetric stretching (ν_s), and out of plane bending. The actual vibrational modes are likely much more complicated due to coupling of the adsorbate and substrate vibrations, but this simple intuitive picture provides valuable insight regarding the dipole-activity of the two cases. In the case of the epoxide group, the asymmetric and symmetric stretching vibrations induce a dynamical dipole moment (DDM) that has a component normal to the basal planes,

while in the case of the ether group, the asymmetric and symmetric stretches both involve only displacements within the basal plane. Thus, a measurement that is only sensitive to out-of-plane atomic displacements can differentiate vibrations from the two functional groups.

We performed such a measurement by employing the grazing incidence reflectance (GIR) geometry using p-polarized radiation. In this case, the sample was deposited on a gold substrate, which was used as the reference measurement. The presence of the metal substrate imposes selection rules such that only vibrations that induce a DDM with a component normal to the surface are activated. In addition, the use of p-polarized radiation and GI ensure that the electric field just above the metal surface is normal to the surface. Fig. 3C shows the resulting absorption spectrum from the GIR measurement. As with the transmission measurement, an intense mode is observed in the 1200 cm^{-1} region that appears to be a superposition of several modes and spans the frequency region 1075–1300 cm^{-1}. Importantly, the C=C stretching feature is not observed, indicating that the metal substrate and GI geometry have effectively suppressed the IR activity of the strictly in-plane vibrations. Thus, the 1200 cm^{-1} feature must be associated with a vibration(s) involving out-of-plane atomic displacements. The absence of any other features in the spectrum strongly suggests that this mode can only be attributed to an epoxide species.

If indeed this feature is due to an epoxide, two modes would be expected; one from symmetric and the other from asymmetric stretching. To confirm the presence of both modes, we performed transmission measurements with polarized radiation. The microscope optic used has a numerical aperture of 0.65, meaning that the radiation illuminates the sample at off-normal incidence. Because synchrotron beams are employed as the light source, the sample is effectively illuminated at off-normal incidence by a low-emittance beam (similar to a laser). By using polarizers upstream of the sample, we can effectively select the s and p-polarized components of the incident beam. Fig. 4 shows absorbance spectra taken at 2 orthogonal polarizations, which effectively emphasize the s and p components of the beam, and 1 polarization at 45° with respect to the orthogonal polarizations. Using this approach, the two modes become spectrally resolved.

In the case of the s-polarized absorbance, the peak position is observed at 1235 cm^{-1}. As the s-polarized radiation only excites vibrations that have a DDM-component parallel to the basal planes, this feature is assigned to the asymmetric stretching mode. In the case of the p-polarized absorbance spectrum, the apparent band position is shifted to 1180 cm^{-1}, which provides direct evidence that the absorbance in the 1050–1350 cm^{-1} region is due to a superposition of bands. Here, the symmetric stretching mode becomes active in addition to the asymmetric stretching mode, both of which overlap to produce a single absorption band. The symmetric stretching band is centered at 1165 cm^{-1}, which is also apparent in the 45° spectrum. We note that the evidence presented does not unequivocally prove that both the 1180 and 1235 cm^{-1} bands originate from the same chemical species; however, both ether and epoxide species necessarily both possess symmetric and asymmetric C-O-C stretching modes which are typically found in the 1000–1400 cm^{-1} spectral region.[49] Since at least one observed mode involves an out-of-plane DDM, it is reasonable to conclude that this mode arises from an epoxide and that indeed epoxide groups are present in appreciable quantities. This does not, however, exclude the possibility that edge ether groups are present and absorbing in the same spectral region assigned to the epoxide asymmetric stretching mode. It is in fact likely these groups are present as well and contribute some intensity in the complex absorption profile observed in the spectra in Fig. 4A, particularly in light of published DFT modeling predicting such contributions in this frequency region.[27]

The absorbance of RGO also suggests a gap is present in the JDOS. Here the position of the gap is somewhat obscured by inhomogeneous broadening, but an approximate value can still

be extracted by calculating the square of the broadband absorbance and finding the intercept. This approach yields a gap of ≈0.19 eV. It is reasonable to ask whether the multilayer morphology of the RGO films could impact the electronic structure and our assessment of the presence of a band gap. We note, however, that these samples are deposited from solution and consequently are rotationally disordered. It has been shown that such rotational disorder leads to a decoupling of the graphene layers,[50] such that the electronic structure of each individual layer is effectively that of an isolated layer.

The difference in the magnitude of the gap between RGO and epitaxial graphene epoxide is relatively small, and could arise from the different degree of ordering in EG and RGO, different epoxide coverages, and interactions with the SiC substrate. The largest and most unexpected difference between the two materials is in the frequency of the C-O-C peak, which is offset by approximately 50 cm^{-1} between the two samples (1285 cm^{-1} *vs* 1235 cm^{-1} for graphene epoxide and RGO, respectively). The blueshifted frequency in the case of EG could occur because of the presence of the polar SiC surface termination, which produces an electric field normal to the surface. This increases the effective field that is felt by the epoxide oxygen, and could increase its vibrational frequency, similar to the dipole-dipole effect that increases the vibrational frequencies of adsorbed molecules[51]. Another possibility is that chemical effects related to the overall oxygen coverage and the position of the Fermi level relative to the adsorbate resonances are responsible for the difference in frequency. More controlled studies with varying coverages are needed to thoroughly understand the origin of the frequency shift in the two cases.

In summary, we have studied epoxide groups on graphene in two systems, EG and RGO. In both cases, broadband spectral lineshapes suggest the presence of a band gap and a distortion of the linear dispersion expected for pure graphene induced by the chemical bonding of epoxides. This is a highly significant result, as it clearly demonstrates a controllable means for chemical band-gap engineering and suggest that controlled oxidation may be a promising direction for manipulating the electronic properties of graphene-based materials.

Methods

Epitaxial graphene samples were grown on n-type 4H-SiC(0001) wafers from Cree Inc. by annealing in an ultra-high vacuum (UHV) chamber at 1270 °C for 15 minutes. Controlled oxidation of the epitaxial graphene samples was achieved by cracking 2×10^{-6} torr O_2 using a hot tungsten filament operating at ≈1500 °C and located 7 cm in front of the sample. As a reference for the IR measurements, a clean $6\sqrt{3} \times 6\sqrt{3}$ reconstructed SiC(0001) substrate was prepared by annealing to 1100°C in UHV. In the time between sample preparation, transportation, and measurement, the samples were stored in a gate valve that was pumped down to 10^{-7} torr.

RGO suspensions were reduced via hydrazine treatment and resuspended in *N*,*N*-dimethylformamide as described previously.[48] The samples were prepared for IR measurements by drop-casting the resulting suspension onto an appropriate substrate (described below), followed by 150° C annealing in air for 1 hour to remove any residual solvent.

IR Microspectroscopy experiments were performed at the Synchrotron Radiation Center using the Infrared Environmental Imaging (IRENI) beamline.[52, 53] The beamline extracts all of the radiation from a synchrotron bending magnet (320 mrad horizontally by 27 mrad vertically) to produce 12 independent synchrotron beams. The beamline uses a Bruker Vertex 70 IR spectrometer and a Bruker Hyperion 3000 IR microscope equipped with a

mercury cadmium telluride (MCT) single-point detector. Several experimental geometries were employed; the graphene/SiC(0001) samples were measured at near-normal incidence reflection using a 36× magnification objective with a numerical aperture (NA) of 0.5. RGO samples deposited onto Au substrates were measured in reflection at grazing incidence using a 15× Bruker grazing angle objective. RGO samples deposited onto diamond substrates were measured in transmission using a 74× (NA=0.65) magnification objective. Polarization, when used, was achieved with an IR wire grid polarizer. All of the measurements were performed at room temperature with the sample in a nitrogen purge box.

Supplementary Material

Refer to Web version on PubMed Central for supplementary material.

Acknowledgments

The authors acknowledge support from the National Science Foundation, awards CMMI-0856753 and CMMI-0900509. This work was performed at the Synchrotron Radiation Center, which is supported by the University of Wisconsin-Madison and the University of Wisconsin-Milwaukee. The IRENI beamline was developed with the support of an NSF major research instrumentation award, DMR-0619759. J.E.J acknowledges an IIN Postdoctoral Fellowship and the Northwestern University International Institute for Nanotechnology, as well as the National Institutes of Health and National Institute of Arthritis and Musculoskeletal and Skin Diseases (NIH/NIAMS T32 AR007611). M.C.H. acknowledges funding from the Office of Naval Research (Award Number N00014-11-1-0463), and a W. M. Keck Foundation Science and Engineering Grant.

References

1. Novoselov KS, Geim AK, Morozov SV, Jiang D, Zhang Y, Dubonos SV, Grigorieva IV, Firsov AA. Electric Field Effect in Atomically Thin Carbon Films. Science. 2004; 306:666–669. [PubMed: 15499015]
2. Novoselov KS, Geim AK, Morozov SV, Jiang D, Katsnelson MI, Grigorieva IV, Dubonos SV, Firsov AA. Two-dimensional Gas of Massless Dirac Fermions in Graphene. Nature. 2005; 438:197–200. [PubMed: 16281030]
3. Zhang YB, Tan YW, Stormer HL, Kim P. Experimental Observation of the Quantum Hall Effect and Berry's Phase in Graphene. Nature. 2005; 438:201–204. [PubMed: 16281031]
4. Castro Neto AH, Guinea F, Peres NMR, Novoselov KS, Geim AK. The Electronic Properties of Graphene. Rev Mod Phys. 2009; 81:109–162.
5. Hossain MZ, Johns JE, Bevan KH, Karmel HJ, Liang YT, Yoshimoto S, Mukai K, Koitaya T, Yoshinobu J, Kawai M, et al. Chemically Homogeneous and Thermally Reversible Oxidation of Epitaxial Graphene. Nat Chem. 2012; 4:305–309. [PubMed: 22437716]
6. Johns JE, Hersam MC. Atomic Covalent Functionalization of Graphene. Acc Chem Res. 2013; 46:77–86. [PubMed: 23030800]
7. Gyamfi M, Eelbo T, Wasniowska M, Wehling TO, Forti S, Starke U, Lichtenstein AI, Katsnelson MI, Wiesendanger R. Orbital Selective Coupling between Ni Adatoms and Graphene Dirac Electrons. Phys Rev B. 2012; 85
8. Mattson EC, Pande K, Unger M, Cui SM, Lu GH, Gajdardziska-Josifovska M, Weinert M, Chen JH, Hirschmugl CJ. Exploring Adsorption and Reactivity of NH3 on Reduced Graphene Oxide. J Phys Chem C. 2013; 117:10698–10707.
9. Williams G, Seger B, Kamat PV. TiO2-graphene Nanocomposites. UV-assisted Photocatalytic Reduction of Graphene Oxide. ACS Nano. 2008; 2:1487–1491. [PubMed: 19206319]
10. Wen ZH, Cui SM, Kim HJ, Mao S, Yu KH, Lu GH, Pu HH, Mao O, Chen JH. Binding Sn-based Nanoparticles on Graphene as the Anode of Rechargeable Lithium-ion Batteries. J Mater Chem. 2012; 22:3300–3306.
11. Lu GH, Mao S, Park S, Ruoff RS, Chen JH. Facile, Noncovalent Decoration of Graphene Oxide Sheets with Nanocrystals. Nano Res. 2009; 2:192–200.

12. Song YM, Yoon M, Jang SY, Jang DM, Cho YJ, Kim CH, Park J, Cha EH. Size and Phase Controlled Synthesis of CdSe/ZnS Core/Shell Nanocrystals Using Ionic Liquid and Their Reduced Graphene Oxide Hybrids as Promising Transparent Optoelectronic Films. J Phys Chem C. 2011; 115:15311–15317.
13. Wang QH, Hersam MC. Room-temperature Molecular-resolution Characterization of Self-assembled Organic Monolayers on Epitaxial Graphene. Nat Chem. 2009; 1:206–211. [PubMed: 21378849]
14. Tang SB, Cao ZX. Adsorption and Dissociation of Ammonia on Graphene Oxides: A First-Principles Study. J Phys Chem C. 2012; 116:8778–8791.
15. Yan JA, Xian LD, Chou MY. Structural and Electronic Properties of Oxidized Graphene. Phys Rev Lett. 2009; 103
16. Yan JA, Chou MY. Oxidation Functional Groups on Graphene: Structural and Electronic Properties. Phys Rev B. 2010; 82
17. Pu HH, Rhim SH, Hirschmugl CJ, Gajdardziska-Josifovska M, Weinert M, Chen JH. Strain-induced Band-gap Engineering of Graphene Monoxide and its Effect on Graphene. Phys Rev B. 2013; 87
18. Johns JE, Alaboson JMP, Patwardhan S, Ryder CR, Schatz GC, Hersam MC. Metal Oxide Nanoparticle Growth on Graphene via Chemical Activation with Atomic Oxygen. J Am Chem Soc. 2013; 135:18121–18125. [PubMed: 24206242]
19. Stankovich S, Dikin DA, Dommett GHB, Kohlhaas KM, Zimney EJ, Stach EA, Piner RD, Nguyen ST, Ruoff RS. Graphene-based Composite Materials. Nature. 2006; 442:282–286. [PubMed: 16855586]
20. Dikin DA, Stankovich S, Zimney EJ, Piner RD, Dommett GHB, Evmenenko G, Nguyen ST, Ruoff RS. Preparation and Characterization of Graphene Oxide Paper. Nature. 2007; 448:457–460. [PubMed: 17653188]
21. Stankovich S, Dikin DA, Piner RD, Kohlhaas KA, Kleinhammes A, Jia Y, Wu Y, Nguyen ST, Ruoff RS. Synthesis of Graphene-based Nanosheets via Chemical Reduction of Exfoliated Graphite Oxide. Carbon. 2007; 45:1558–1565.
22. Daas BK, Daniels KM, Sudarshan TS, Chandrashekhar MVS. Polariton Enhanced Infrared Reflection of Epitaxial Graphene. J App Phys. 2011; 110
23. Kuzmenko AB, Benfatto L, Cappelluti E, Crassee I, van der Marel D, Blake P, Novoselov KS, Geim AK. Gate Tunable Infrared Phonon Anomalies in Bilayer Graphene. Phys Rev Lett. 2009; 103
24. Cappelluti E, Benfatto L, Kuzmenko AB. Phonon Switching and Combined Fano-Rice Effect in Optical Spectra of Bilayer Graphene. Phys Rev B. 2010; 82
25. Tang TT, Zhang YB, Park CH, Geng BS, Girit C, Hao Z, Martin MC, Zettl A, Crommie MF, Louie SG, et al. A Tunable Phonon-exciton Fano System in Bilayer Graphene. Nat Nanotechnol. 2010; 5:32–36. [PubMed: 19915569]
26. Mattson EC, Pu HH, Cui SM, Schofield MA, Rhim S, Lu GH, Nasse MJ, Ruoff RS, Weinert M, Gajdardziska-Josifovska M, et al. Evidence of Nanocrystalline Semiconducting Graphene Monoxide during Thermal Reduction of Graphene Oxide in Vacuum. ACS Nano. 2011; 5:9710–9717. [PubMed: 22098501]
27. Acik M, Lee G, Mattevi C, Pirkle A, Wallace RM, Chhowalla M, Cho K, Chabal Y. The Role of Oxygen during Thermal Reduction of Graphene Oxide Studied by Infrared Absorption Spectroscopy. J Phys Chem C. 2011; 115:19761–19781.
28. Bagri A, Mattevi C, Acik M, Chabal YJ, Chhowalla M, Shenoy VB. Structural Evolution During the Reduction of Chemically Derived Graphene Oxide. Nat Chem. 2010; 2:581–587. [PubMed: 20571578]
29. Acik M, Lee G, Mattevi C, Chhowalla M, Cho K, Chabal YJ. Unusual Infrared-absorption Mechanism in Thermally Reduced Graphene Oxide. Nat Mater. 2010; 9:840–845. [PubMed: 20852618]
30. Zhou SY, Gweon GH, Fedorov AV, First PN, De Heer WA, Lee DH, Guinea F, Neto AHC, Lanzara A. Substrate-induced Bandgap Opening in Epitaxial Graphene. Nat Mater. 2007; 6:770–775. [PubMed: 17828279]

31. Bostwick A, Ohta T, Seyller T, Horn K, Rotenberg E. Quasiparticle Dynamics in Graphene. Nat Phys. 2007; 3:36–40.
32. Kuzmenko AB. Kramers-Kronig Constrained Variational Analysis of Optical Spectra. Rev Sci Instrum. 2005; 76
33. Li ZQ, Henriksen EA, Jiang Z, Hao Z, Martin MC, Kim P, Stormer HL, Basov DN. Dirac Charge Dynamics in Graphene by Infrared Spectroscopy. Nat Phys. 2008; 4:532–535.
34. Mak KF, Sfeir MY, Wu Y, Lui CH, Misewich JA, Heinz TF. Measurement of the Optical Conductivity of Graphene. Phys Rev Lett. 2008; 101
35. Rotenberg E, Bostwick A, Ohta T, McChesney JL, Seyller T, Horn K. Origin of the Energy Bandgap in Epitaxial Graphene. Nat Mater. 2008; 7:258–259. [PubMed: 18354403]
36. Qi Y, Rhim SH, Sun GF, Weinert M, Li L. Epitaxial Graphene on SiC(0001): More than Just Honeycombs. Phys Rev Lett. 2010; 105
37. Dressel, M.; Grüner, G. Electrodynamics of Solids: Optical Properties of Electrons in Matter. Cambridge University Press; Cambridge, UK: 2002.
38. Geim AK, Novoselov KS. The Rise of Graphene. Nat Mater. 2007; 6:183–191. [PubMed: 17330084]
39. Kuzmenko AB, van Heumen E, Carbone F, van der Marel D. Universal Optical Conductance of Graphite. Phys Rev Lett. 2008; 100
40. Zhou SY, Siegel DA, Fedorov AV, Lanzara A. Metal to Insulator Transition in Epitaxial Graphene Induced by Molecular Doping. Phys Rev Lett. 2008; 101
41. Zhang YB, Tang TT, Girit C, Hao Z, Martin MC, Zettl A, Crommie MF, Shen YR, Wang F. Direct Observation of a Widely Tunable Bandgap in Bilayer Graphene. Nature. 2009; 459:820–823. [PubMed: 19516337]
42. Sjovall P, So SK, Kasemo B, Franchy R, Ho W. NO_2 Adsorption on Graphite at 90-K. Chem Phys Lett. 1990; 172:125–130.
43. Eda G, Fanchini G, Chhowalla M. Large-area Ultrathin Films of Reduced Graphene Oxide as a Transparent and Flexible Electronic Material. Nat Nanotechnol. 2008; 3:270–274. [PubMed: 18654522]
44. Mao S, Lu GH, Yu KH, Bo Z, Chen JH. Specific Protein Detection Using Thermally Reduced Graphene Oxide Sheet Decorated with Gold Nanoparticle-Antibody Conjugates. Adv Mater. 2010; 22:3521. [PubMed: 20665564]
45. Cui S, Wen Z, Mattson EC, Mao S, Chang J, Weinert M, Hirschmugl CJ, Gajdardziska-Josifovska M, Chen J. Indium-doped SnO2 Nanoparticle-graphene Nanohybrids: Simple One-pot Synthesis and their Selective Detection of NO2. J Mater Chem A. 2013; 1:4462–4467.
46. Kaniyoor A, Baby TT, Ramaprabhu S. Graphene Synthesis via Hydrogen Induced Low Temperature Exfoliation of Graphite Oxide. J Mater Chem. 2010; 20:8467–8469.
47. Zhu J, Andres CM, Xu JD, Ramamoorthy A, Tsotsis T, Kotov NA. Pseudonegative Thermal Expansion and the State of Water in Graphene Oxide Layered Assemblies. ACS Nano. 2012; 6:8357–8365. [PubMed: 22861527]
48. Park S, An JH, Jung IW, Piner RD, An SJ, Li XS, Velamakanni A, Ruoff RS. Colloidal Suspensions of Highly Reduced Graphene Oxide in a Wide Variety of Organic Solvents. Nano letters. 2009; 9:1593–1597. [PubMed: 19265429]
49. Nakamoto, K. Infrared and Raman Spectra of Inorganic and Coordination Compounds. John Wiley & Sons, Inc; Hoboken, NJ: 2008.
50. Hass J, Varchon F, Millan-Otoya JE, Sprinkle M, Sharma N, De Heer WA, Berger C, First PN, Magaud L, Conrad EH. Why Multilayer Graphene on 4H-SiC(000(1)over-bar) Behaves like a Single Sheet of Graphene. Phys Rev Lett. 2008; 100
51. Persson BNJ, Ryberg R. Vibrational Interaction between Molecules Adsorbed on a Metal Surface: The Dipole-dipole Interaction. Phys Rev B. 1981; 24:6954–6970.
52. Nasse MJ, Walsh MJ, Mattson EC, Reininger R, Kajdacsy-Balla A, Macias V, Bhargava R, Hirschmugl CJ. High-resolution Fourier-transform Infrared Chemical Imaging with Multiple Synchrotron Beams. Nat Methods. 2011; 8:413–U58. [PubMed: 21423192]

53. Nasse MJ, Mattson EC, Reininger R, Kubala T, Janowski S, El-Bayyari Z, Hirschmugl CJ. Multi-beam Synchrotron Infrared Chemical Imaging with High Spatial Resolution: Beam line Realization and First Reports on Image Restoration. Nucl Instrum Methods Phys Res Sect A-Accel Spectrom Dect Assoc Equip. 2011; 649:172–176.

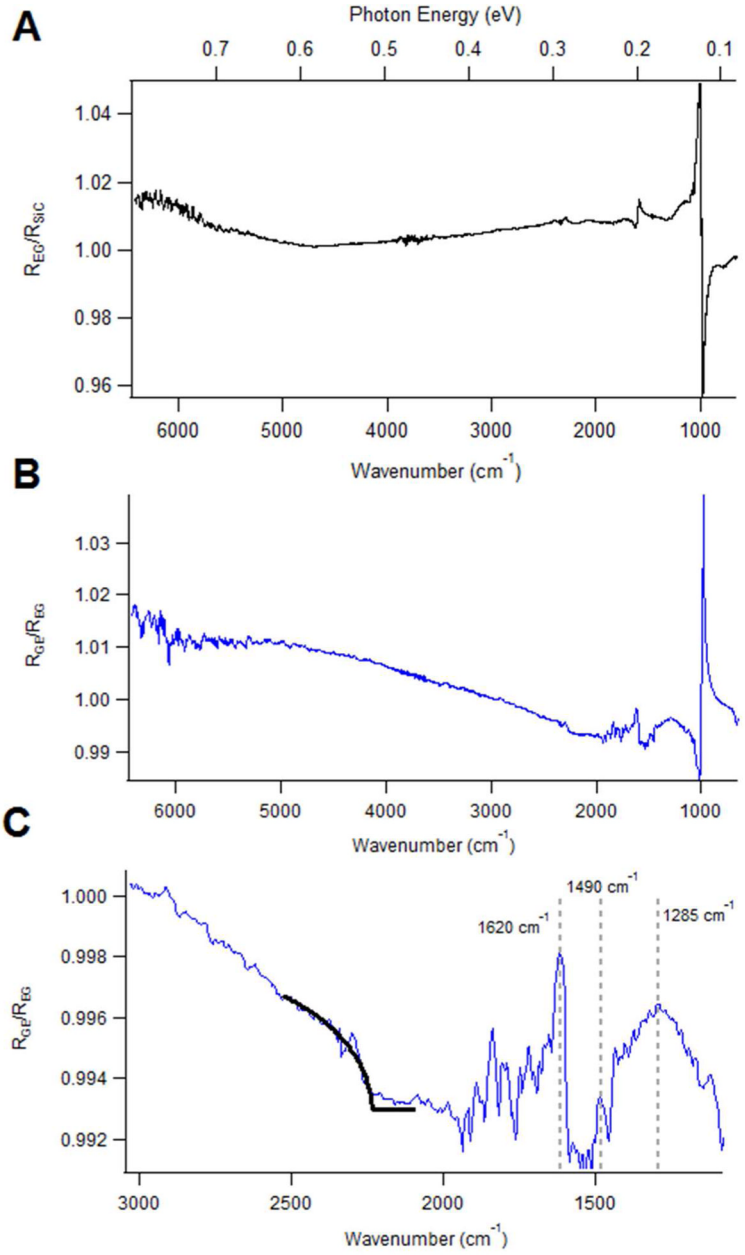

Figure 1.

A) IR difference reflectivity of EG/SiC(0001) referenced to the $6\sqrt{3} \times 6\sqrt{3}$ SiC(0001). B) IR reflectivity of GE referenced to clean EG, with the region between 1000–3000 cm^{-1} expanded in C), and a black curve indicating the behavior around an M_o critical point in the JDOS is overlaid.

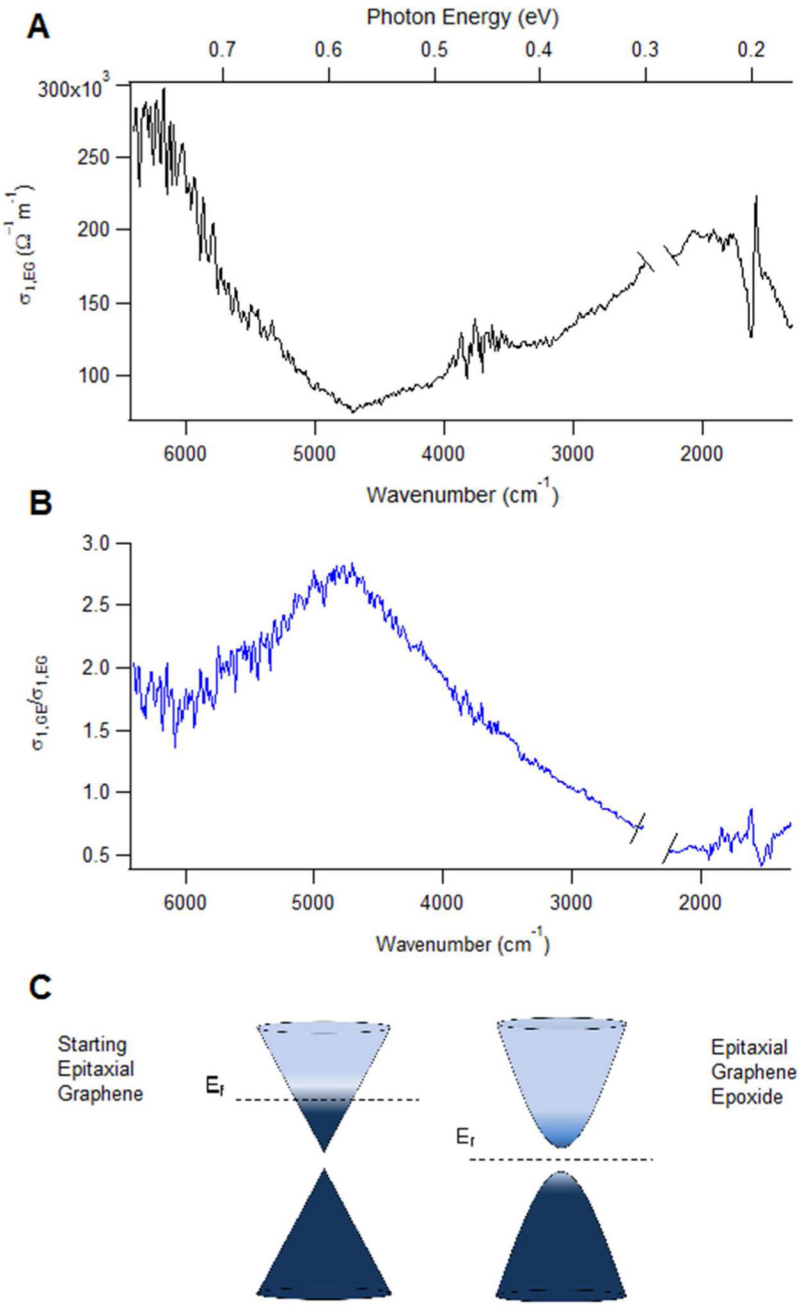

Figure 2.

A) Real part of the extracted optical conductivity of the EG layer from Fig. 1A. The region from 2300–2400 cm^{-1} has been removed due to the incomplete cancellation of CO_2 in this region, which produces a large artifact in the conductivity. B) Real part of the optical conductivity of the GE sample referenced to that of the EG sample. C) Schematic diagram of the occupation of the π bands around the K-point in clean EG (left) and GE (right). In both cases there is a small gap at the K-point, but in the oxidized sample the band dispersion is distorted from linear to parabolic, and the Fermi level has been lowered such that the gap is accessible to optical measurements.

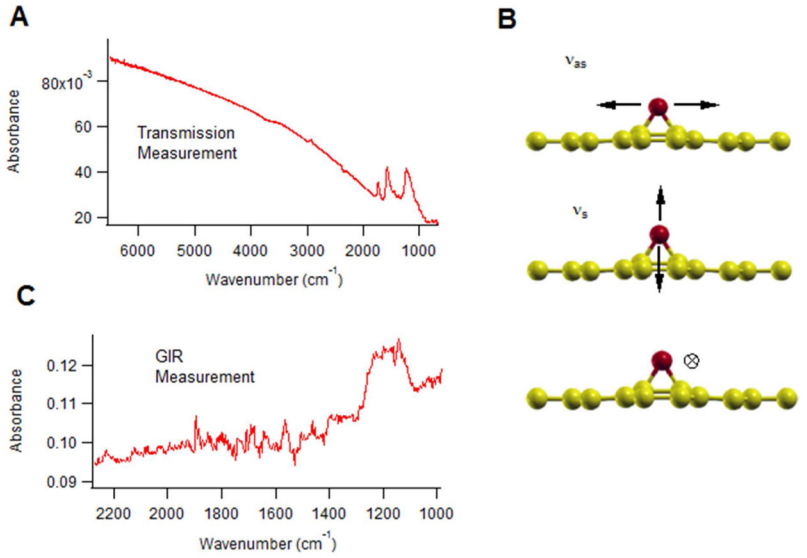

Figure 3.

A) IR absorbance of RGO determined from transmission measurements using an objective with NA=0.65. B) Simplified models of the normal modes of an epoxide group on a frozen substrate. In reality, the asymmetric stretching mode (top) also involves a perpendicular displacement of both the oxygen and carbon atoms in the epoxide group. C) IR absorbance of RGO determined in the GI reflection geometry using p-polarized radiation.

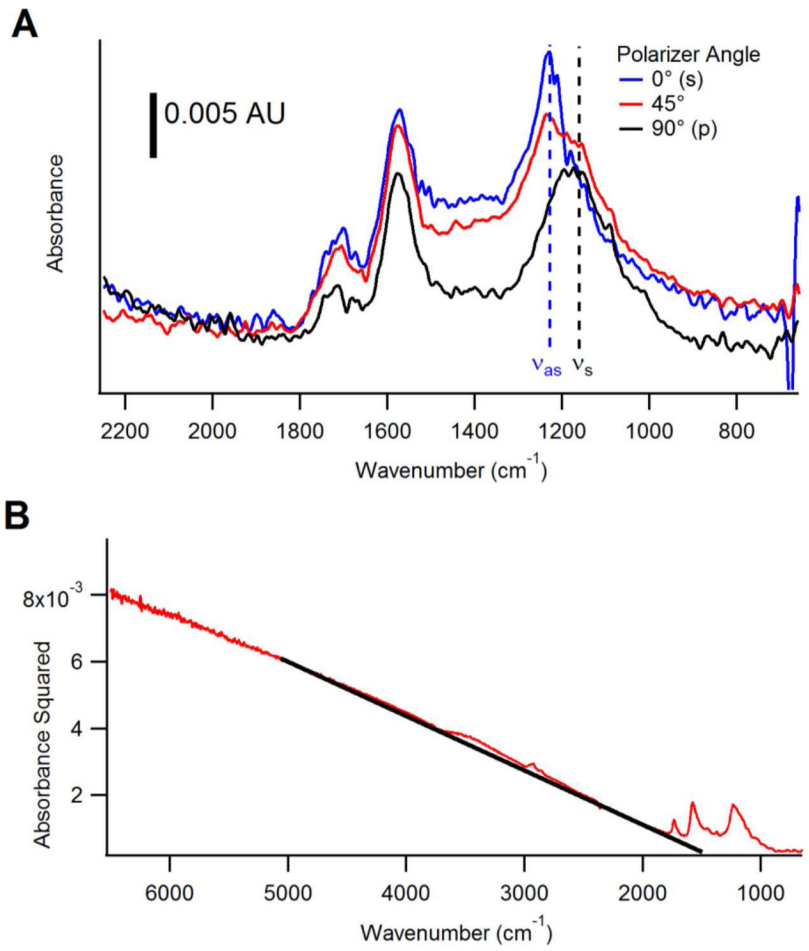

Figure 4.

A) Absorption spectra of RGO determined from transmission measurements with different polarizations. The polarizer angle effectively selects s and p-polarization, and one intermediate polarization is also shown. The symmetric and asymmetric modes from Fig. 3 are labeled as ν_s and ν_{as}, respectively. B) Square of the absorbance of RGO (unpolarized spectrum from Fig. 3A) overlaid with a linear dependence to show the intercept at 1500 cm^{-1}.